Supercooled Liquids under Shear: Computational Approach

Ryoichi Yamamoto

Department of Physics, Kyoto University, Kyoto 606-8502, Japan, and
PRESTO, Japan Science and Technology Agency, 4-1-8 Honcho, Kawaguchi, Saitama, Japan

Abstract. We examine the microscopic dynamics of supercooled liquids under shear by performing extensive molecular dynamics simulations of a two-dimensional binary liquid with soft-core interactions near, but above, the glass transition temperature. Our simulations show that a drastic reduction of the structural relaxation time and the shear viscosity occurs due to shear. The structural relaxation time decreases as $\dot{\gamma}^{-\nu}$ with an exponent $\nu \leq 1$, where $\dot{\gamma}$ is the shear rate. The microscopic dynamics were confirmed to be surprisingly isotropic regardless of the strength of the anisotropic shear flow.

1 Introduction

As liquids are cooled toward the glass transition, the dynamics are drastically slowed down, while only small changes can be detected in the static properties. One of the main targets of theoretical investigations of the glass transition is to identify the mechanism of this drastic slowing-down. To this end, a number of molecular dynamics (MD) simulations have been carried out for supercooled liquids and revealed that the dynamics in supercooled liquids are spatially *heterogeneous*[1–10]. In our previous studies, we have examined bond breakage processes among adjacent particle pairs by MD simulations of two (2D) and three dimensional (3D) model fluids. We found that the broken bonds determined with an appropriate time interval ($\simeq 0.05\tau_b$, where τ_b is the average bond breakage time), are almost equivalent to the critical fluctuations in Ising spin systems. To support this picture, the structure factor of the broken bonds can be excellently fit to the Ornstein-Zernike form.[4,5] The correlation length ξ determined from this analysis increases with decreasing temperature T and is related to τ_b or the structural α relaxation time τ_α via the dynamic scaling law, $\tau_\alpha \simeq 0.1\tau_b \sim \xi^z$, with $z = 4$ in 2D and $z = 2$ in 3D. The heterogeneous structure of the bond breakage is essentially the same as that in local diffusivity.[6]

Another striking example occurs when one brings supercooled liquids away from equilibrium. By rapidly changing the temperature or applying shear flow, supercooled liquids undergo unique phenomena known as aging or shear thinning [11–15]. These phenomena are not only conceptually new but also practically important. However, physical properties of glassy materials have not yet been well-understood in nonequilibrium conditions. In

previous work, we performed extensive MD simulations of binary soft-core mixtures in two and three dimensions with and without shear flow. We found that the dynamical properties of the supercooled liquids under shear can be mapped onto those at quiescent states at higher temperatures [5]. In the present study, we calculate intermediate scattering functions in shear flow by using a method proposed by Onuki [17,18] to examine the microscopic dynamics of sheared supercooled liquids. Simulations have been done in 2D to compare the present computational results directly with a theory developed recently for sheared supercooled liquids in 2D [19,20].

2 Simulation method

To prevent crystallization and obtain stable amorphous states via MD simulations, we choose a model system composed of two different particle species, 1 and 2, which interact via the soft-core potential

$$v_{ab}(r) = \epsilon(\sigma_{ab}/r)^{12}, \tag{1}$$

with $\sigma_{ab} = (\sigma_a + \sigma_b)/2$, where r is the distance between the two particles, and a, b denote particle species ($\in \{1, 2\}$). We take the mass ratio to be $m_2/m_1 = 2$, the size ratio to be $\sigma_2/\sigma_1 = 1.4$, and the number of particles $N = N_1 + N_2$, where $N_1 = N_2 = 5000$. Simulations are performed in the presence and absence of shear flow keeping the particle density and the temperature fixed at $n = n_1 + n_2 = 0.8/\sigma_1^2$ ($n_1 = N_1/V$, $n_2 = N_2/V$) and $k_BT = 0.526\epsilon$. Space and time are measured in units of σ_1 and $\tau_0 = (m_1\sigma_1^2/\epsilon)^{1/2}$, respectively. The size of the unit cell is $L = 118$. In the absence of shear, we impose microcanonical conditions and integrate Newton's equations of motion

$$\frac{d\mathbf{r}_i^a}{dt} = \frac{\mathbf{p}_i^a}{m_a}, \quad \frac{d\mathbf{p}_i^a}{dt} = \mathbf{f}_i^a. \tag{2}$$

Very long equilibration periods are used so that no appreciable aging (slow equilibration) effect is detected in various thermodynamic quantities, such as the pressure, or in time correlation functions. Here, $\mathbf{r}_i^a = (r_{xi}^a, r_{yi}^a)$ and $\mathbf{p}_i^a = (p_{xi}^a, p_{yi}^a)$ denote the position and the momentum of the i-th particle of species a, and $\mathbf{f}_i^a$ is the force acting on the i-th particle of species a. In the presence of shear, the momentum $\mathbf{p'}_i^a = \mathbf{p}_i^a - m_a\dot{\gamma}r_{yi}^a\hat{\mathbf{e}}_x$ is defined as the momentum deviations relative to mean Couette flow. Using the Lee-Edwards boundary condition, we integrate the so-called SLLOD equations of motion keeping the temperature k_BT ($\equiv N^{-1}\sum_a\sum_i(\mathbf{p'}_i^a)^2/m_a$) at a desired value using a Gaussian-constraint thermostat to eliminate viscous heating effects[21]. We impose shear for $t \geq 0$ after a long equilibriation time. Data for the analysis has been taken and accumulated in steady states which can be realized after transient waiting periods.

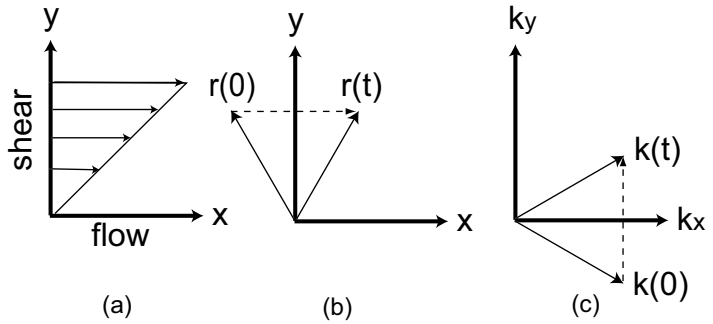

Fig. 1. (a) Geometry of shear flow. (b) Shear advection in real space. (c) Shear advection in Fourier space.

Figure 1 (a) shows the geometry of shear flow in the present simulation. As shown in Fig.1 (b), shear flow with the rate $\dot{\gamma}$ advect a positional vector $\mathbf{r}$ as

$$\mathbf{r}(t) = \mathbf{r} + \dot{\gamma} t r_y \mathbf{e}_x, \tag{3}$$

for time t, where $\mathbf{e}_\alpha$ is a unit vector in $\alpha \in \{x, y\}$ axis. The corresponding time-dependent wave vector

$$\mathbf{k}(t) = \mathbf{k} + \dot{\gamma} t k_x \mathbf{e}_y, \tag{4}$$

is shown in Fig.1 (c). The above definition enable us to calculate the Fourier component $\mathbf{k}$ of the time correlation function

$$C(\mathbf{k}, t) \equiv \langle A_{-\mathbf{k}(t)}(t) A_{\mathbf{k}}(0) \rangle \tag{5}$$

in shear flow [17,18]. We thus calculate the incoherent and the coherent parts of the scattering function for the binary mixture using the definitions [22]

$$F_{sa}(\mathbf{k}, t) = \frac{1}{N_a} \left\langle \sum_{i=1}^{N_a} \mathrm{e}^{[-i\{\mathbf{k}(-t)\cdot\mathbf{r}_i^a(t) - \mathbf{k}\cdot\mathbf{r}_i^a(0)\}]} \right\rangle \tag{6}$$

and

$$F_{ab}(\mathbf{k}, t) = \frac{1}{N} \left\langle \sum_{i=1}^{N_a} \mathrm{e}^{[-i\mathbf{k}(-t)\cdot\mathbf{r}_i^a(t)]} \sum_{j=1}^{N_b} \mathrm{e}^{[i\mathbf{k}\cdot\mathbf{r}_j^b(0)]} \right\rangle, \tag{7}$$

with $a, b \in \{1, 2\}$. The α relaxation time τ_α of the present mixture, defined by

$$F_{11}(\mathbf{k}_0, \tau_\alpha) \simeq F s_1(\mathbf{k}_0, \tau_\alpha) = \mathrm{e}^{-1}, \tag{8}$$

is equal to $\tau_\alpha \simeq 1800$ time units in the quiescent state for $|\mathbf{k}_0| = 2\pi/\sigma_1$.

3 Simulation Results

3.1 Microscopic Structure

The partial static structure factors $S_{ab}(\mathbf{k})$ are defined as

$$S_{ab}(\mathbf{k}) = \int \mathrm{d}\mathbf{r}\ \mathrm{e}^{i\mathbf{k}\cdot\mathbf{r}} \langle \hat{n}_a(\mathbf{r}) \hat{n}_b(\mathbf{0}) \rangle, \tag{9}$$

where

$$\hat{n}_a(\mathbf{r}) = \sum_j^{N_a} \delta(\mathbf{r} - \mathbf{r}_j^a) \qquad (a \in \{1, 2\}), \tag{10}$$

is the local number density of the species a. Note, the dimensionless wave vector $\mathbf{k}$ is measured in units of σ_1^{-1}. For a binary mixture, there are three combinations of partial structure factors, $S_{11}(\mathbf{k})$, $S_{22}(\mathbf{k})$, and $S_{12}(\mathbf{k})$. These are plotted in Fig.2 (a) in the quiescent state after taking an angular average over $\mathbf{k}$. A density variable representing the degree of particle packing, corresponding to the density of an effective one component system, can be defined for the present binary system as

$$\hat{\rho}_{\mathrm{eff}}(\mathbf{r}) = \sigma_1^2 \hat{n}_1(\mathbf{r}) + \sigma_2^2 \hat{n}_2(\mathbf{r}). \tag{11}$$

The corresponding dimensionless structure factor is given by

$$S_{\rho\rho}(\mathbf{k}) = \sigma_1^{-4} \int \mathrm{d}\mathbf{r}\ \mathrm{e}^{i\mathbf{k}\cdot\mathbf{r}} \langle \delta\hat{\rho}_{\mathrm{eff}}(\mathbf{r}) \delta\hat{\rho}_{\mathrm{eff}}(\mathbf{0}) \rangle \tag{12}$$

$$= n_1^2 S_{11}(\mathbf{k}) + n_2^2 (\sigma_2/\sigma_1)^4 S_{22}(\mathbf{k}) + 2 n_1 n_2 (\sigma_2/\sigma_1)^2 S_{12}(\mathbf{k}), \tag{13}$$

where $\delta\hat{\rho}_{\mathrm{eff}} = \hat{\rho}_{\mathrm{eff}} - \langle \hat{\rho}_{\mathrm{eff}} \rangle$. One can see from Fig.2 (b) that $S_{\rho\rho}(k)$ has a pronounced peak at $k \simeq 5.8$ and becomes very small (~ 0.01) for small k, demonstrating that our system is highly incompressible at long wavelengths. Because $S_{\rho\rho}(k)$ behaves quite similarly to $S(k)$ of one component systems, we examine space-time correlations in $\hat{\rho}_{\mathrm{eff}}(\mathbf{r})$ rather than those in the partial number density $\hat{n}_a(\mathbf{r})$ for the present binary system. The use of $\hat{\rho}_{\mathrm{eff}}(\mathbf{r})$ makes comparison of our simulation data with the mode-coupling theory developed for a one component system more meaningful.

We next examine the anisotropy in the static structure factor $S_{\rho\rho}(\mathbf{k})$ in the presence of shear flow. Figures 3 and 4 show $S_{\rho\rho}(\mathbf{k})$ plotted on a two-dimensional $k_x - k_y$ plane (upper part) and the angular averaged curves (lower part) within the regions (a)-(d) obtained at $\dot{\gamma} = 10^{-3}$ and 10^{-2}, respectively. One sees that at a lower shear rate ($\dot{\gamma} = 10^{-3}$), the shear distortion is negligible at all the regions except for region (d) where the peak heights of $S_{\rho\rho}(\mathbf{k})$ start decreasing. But, at higher shear rate ($\dot{\gamma} = 10^{-2}$) the distortion becomes prominent. This seems to indicate that the nonlinear effects due to shear become important in this region. Ronis has explored the higher shear regime for the structure factor of hard sphere colloidal suspensions and concluded

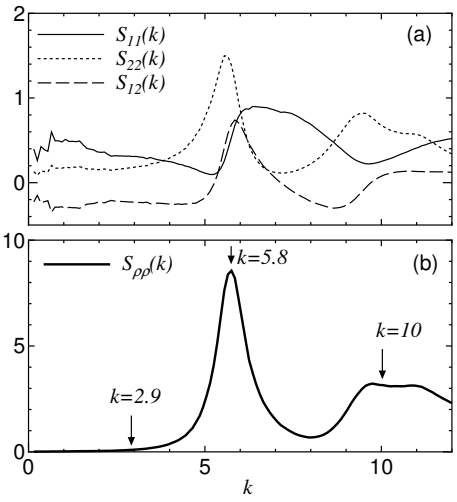

Fig. 2. Partial structure factors $S_{ab}(k)$ in (a) and $S_{\rho\rho}(k)$ in (b) defined by eq.(13) for the present binary mixture.

that, at higher shear, the peak should always be lower than the equilibrium value plus a shift that depends on the direction[23]. At even higher shear rate ($\dot{\gamma} = 10^{-1}$, though the figure is not shown here), peaks in all directions have been lowered. The peak with maximal distortion (region (b)) is shifted to lower wave vectors while the opposite is true for the shift of the region with minimal distortion (region (d)). The qualitative agreement with Ronis' theory is good, but it is not clear that our results can be explained by a simple two-body theory such as that of Ronis. Recently, Szamel has analyzed $S(k)$ for hard-sphere colloidal suspensions up to linear order in $\dot{\gamma}$[24]. He took three-body correlations into account and found quantitative agreement with the shear viscosity evaluated using $S(k)$.

It should be noted that because our system is an atomic liquid without solvent, we cannot directly refer to the Péclet number since the bare diffusion coefficient D_0 does not exist. Therefore, a direct and quantitative comparison with the theories discussed above is not possible. However, we can estimate the relaxation times from the self-diffusion coefficients measured in [5]. This allows us to estimate the Péclet number in the range between 10^{-1} and 10^2, which corresponds to the highest shear rates explored in the theoretical analysis of our paper [20].

3.2 Tagged particle motions

We generalize the displacement vector of the tagged (jth) particle as

$$\Delta \boldsymbol{r}_j(t) = \boldsymbol{r}_j(t) - \dot{\gamma} \int_0^t dt' y_j(t') \boldsymbol{e}_x - \boldsymbol{r}_j(0), \tag{14}$$

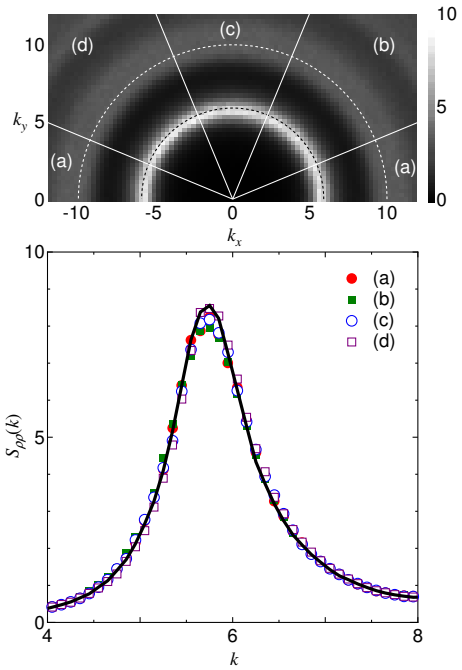

Fig. 3. Upper: $S_{\rho\rho}(\mathbf{k})$ at $\dot{\gamma} = 10^{-3}$ plotted in a two-dimensional $(k_x,\ k_y)$ plane. Lower: The solid line is $S_{\rho\rho}(k)$ at equilibrium. Dots represents those observed in the region indicated in the $(k_x,\ k_y)$ plane above.

where $\boldsymbol{e}_x$ is the unit vector in the x (flow) direction. In this displacement, the contribution from convective transport by the average flow has been subtracted. We then analyze the mean square displacement,

$$r_2(t) \equiv \langle [\Delta \boldsymbol{r}(t)]^2 \rangle = \frac{1}{N_1} \sum_{j=1}^{N_1} \langle [\Delta \boldsymbol{r}_j(t)]^2 \rangle, \tag{15}$$

of tagged particles for the smaller component (species 1). MSDs obtained at $T = 0.53$ with shear rates $10^{-4} \leq \dot{\gamma} \leq 10^{-1}$ are plotted in Fig. 5, where the mean square displacements of the x and y components of the vector $\Delta \boldsymbol{r}_j(t)$ are separately displayed. Analogous to the effect of increasing temperature, the shear flow enhances the mobility of particles. It is also demonstrated that the statistical distribution of $\Delta \boldsymbol{r}_i(t)$ is surprisingly isotropic even at the highest shear rate.

Figure 6 shows the non-Gaussian parameter for the smaller component

$$\alpha_2(t) \equiv 3\langle \Delta \boldsymbol{r}(t)^4 \rangle / 5 \langle \Delta \boldsymbol{r}(t)^2 \rangle^2 - 1, \tag{16}$$

which assumes a maximum value at $t = t^*$. One finds that both t^* and $\alpha_2^* \equiv \alpha_2(t^*)$ tend to decrease with increasing shear rate. This is again analogous to

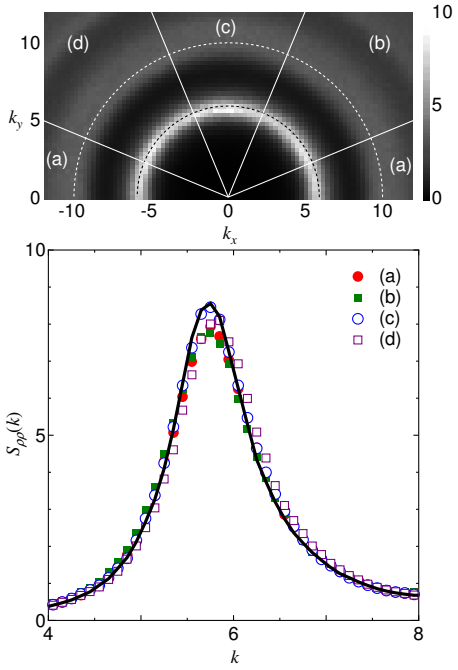

Fig. 4. The same as Fig.3 but shear is increased to $\dot{\gamma} = 10^{-2}$.

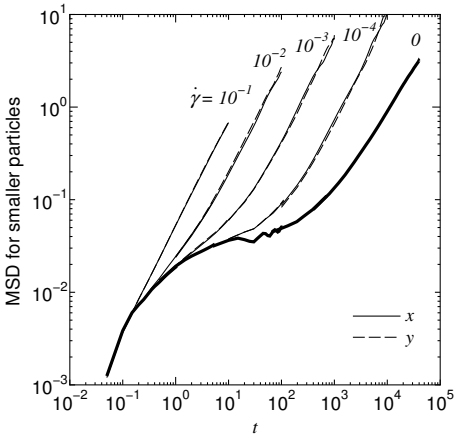

Fig. 5. The mean square displacements (MSD) obtained at $T = 0.53$ under shear flow.

the behavior observed when the temperature is increased without shear flow. A quantative comparison of these two effects (increasing temperature and

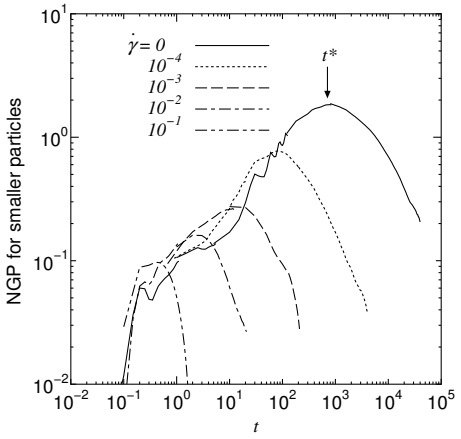

Fig. 6. The non-Gaussian parameter (NGP) obtained at $T = 0.53$ under shear flow.

increasing shear rare) is done in Fig. 7, which supports the analogy between the two effects.

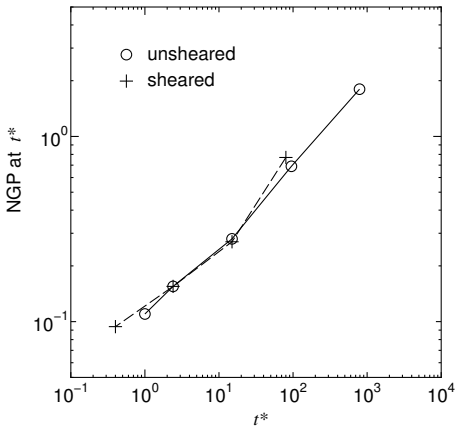

Fig. 7. Peak values of NGP, α_2^*, are plotted against $t*$ at which NGP shows a peak. Data are taken by both changing temperature without shear and changing shear rate at a fixed temperature $T = 0.53$ (+).

We may also conclude that the decrease in NGP^* with increasing temperature or shear rate represents the suppressed heterogeneity, which becomes significant in glassy states.

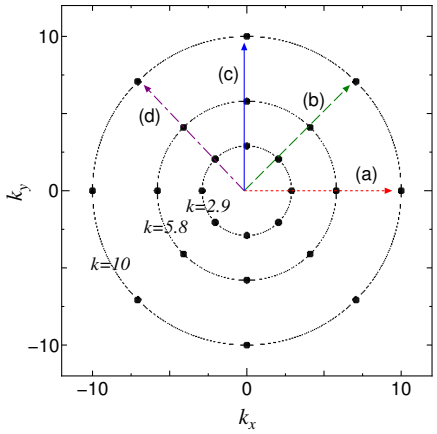

Fig. 8. Sampled wavevectors.

3.3 Intermediate Scattering Functions

Here we examine the dynamics of the local density variable $\hat{\rho}_{\rm eff}(\mathbf{r},t)$. To this end, we define the intermediate scattering function,

$$F_{\rho\rho}(\mathbf{k},t) = n_1^2 F_{11}(\mathbf{k},t)+n_2^2(\sigma_2/\sigma_1)^4 F_{22}(\mathbf{k},t)+2n_1n_2(\sigma_2/\sigma_1)^2 F_{12}(\mathbf{k},t), \quad (17)$$

by taking a linear combination of the partial scattering functions defined in eq.(7). Note that $F_{\rho\rho}(\mathbf{k},0) = S_{\rho\rho}(\mathbf{k})$ by definition. To investigate anisotropy in the scattering function $F_{\rho\rho}(\mathbf{k},t)$, the wave vector $\mathbf{k}$ is taken in four different directions $\mathbf{k}_{10}$, $\mathbf{k}_{11}$, $\mathbf{k}_{01}$, and $\mathbf{k}_{-11}$, where

$$\mathbf{k}_{\mu\nu} = \frac{k}{\sqrt{\mu^2+\nu^2}}(\mu\hat{\mathbf{e}}_x + \nu\hat{\mathbf{e}}_y), \quad (18)$$

and $\mu,\nu \in \{0,1\}$ as shown in Fig.8. The wave vector k (in reduced units) is taken to be 5.8 (see also Fig.2 (b)). Because we use the Lee-Edwards periodic boundary condition, the available wave vectors in our simulations should be given by

$$\mathbf{k} = \frac{2\pi}{L}(n\hat{\mathbf{e}}_x, (m-nD_x)\hat{\mathbf{e}}_y), \quad (19)$$

where n and m are integers and $D_x = L\dot{\gamma}t$ is the difference in x-coordinate between the top and bottom cells as depicted in Fig.6.5 of [21]. To suppress statistical errors, we sample about 80 available wave vectors around $\mathbf{k}_{\mu\nu}$ and calculate $F_{\rho\rho}(\mathbf{k},t)$ using eqs.(17) and (7). Then we average $F_{\rho\rho}(\mathbf{k},t)$ over the sampled wave vectors. The sampled wave vectors are indicated by dots in Fig.8.

Figures 9 displays $F_{\rho\rho}(\mathbf{k},t)/S_{\rho\rho}(\mathbf{k})$ for $k = 5.8$. Several features are noticeable. First, the quantitative trends as a function of k are similar for different values of $\dot{\gamma}$. Secondly, shear drastically accelerates microscopic structural

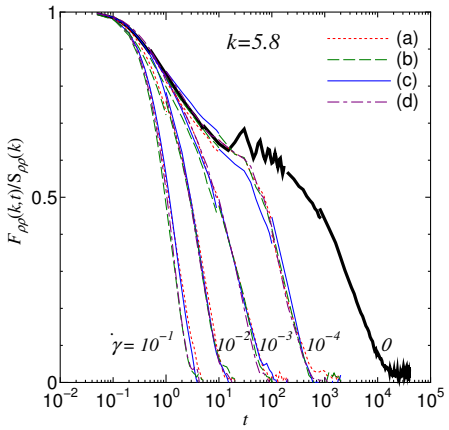

Fig. 9. $F(\mathbf{k},t)/S(\mathbf{k})$ at $k\sigma_1 = 5.8$ for various shear rates and at the different observing points (a) $\mathbf{k}_{10}$, (b) $\mathbf{k}_{11}$, (c) $\mathbf{k}_{01}$, and (d) $\mathbf{k}_{-11}$ as explained in Fig.(8).

relaxation in the supercooled state. The structural relaxation time τ_α decreases strongly with increasing shear rate as $\tau_\alpha \sim \dot{\gamma}^{-\nu}$ with $\nu \simeq 1$ as shown in Fig.10. Thirdly, the acceleration in the dynamics due to shear occurs almost isotropically. Finally, almost the same trend is found for $k = 2.9$ and $k = 10$ as shown in Fig.11. We observe surprisingly small anisotropy in the scattering functions, even under extremely strong shear, $\dot{\gamma}\tau_\alpha \simeq 10^3$. A similar isotropy in the tagged particle motions has already been reported in Fig.5 [5]. The observed isotropy is more surprising than that observed in single particle quantities. In particular, the fact that different particle labels are correlated in the collective quantity defined in eq.(7) means that a simple transformation to a frame moving with the shear flow cannot completely remove the directional character of the shear. Our results provide *post facto* justification for the isotropic approximation of [25]. The observed simplicity in the dynamics is quite different from the behavior of other complex fluids such as critical fluids or polymers, where the dynamics become noticeably anisotropic in the presence of shear flow.

4 Conclusions

We have performed extensive MD simulations for two- and three-dimensional binary liquids with soft-core interactions near, but above, the glass transition temperature. In our previous studies, we identified *weakly-bonded* or *relatively-active* regions from breakage of appropriately defined bonds.[4,5] We also found that the spatial distributions of such regions resemble the critical fluctuations in Ising spin systems, so the correlation length ξ can be determined. The correlation length goes up to the system size as T is lowered, but no divergence seems to exist at nonzero temperatures. We have also

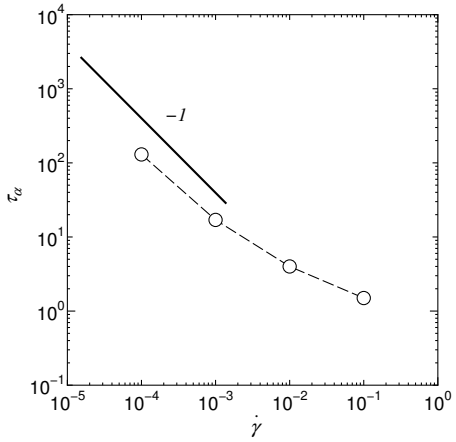

Fig. 10. The alpha relaxation time τ_α at $T = 0.53$ under shear flow. The solid line indicates $\nu = 1$.

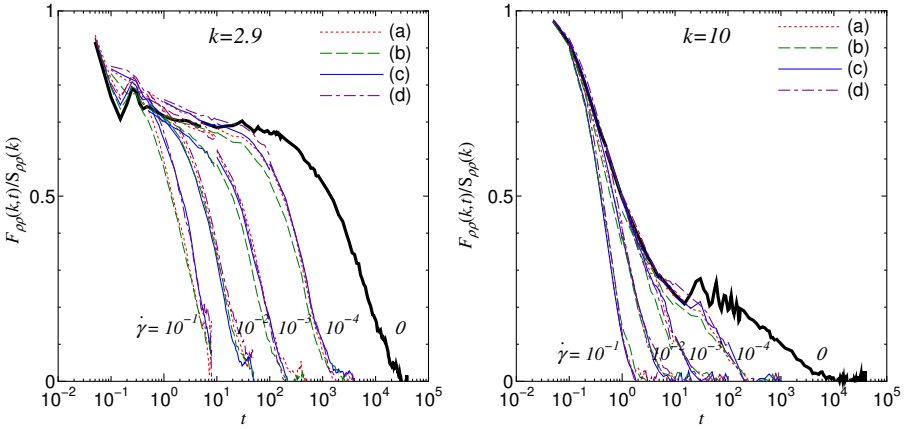

Fig. 11. Left: $F(\mathbf{k},t)/S(\mathbf{k})$ at (a) $k\sigma_1 = 2.9$. Right: $F(\mathbf{k},t)/S(\mathbf{k})$ at $k\sigma_1 = 10$. All symbols are as in Fig.9

demonstrated that the diffusivity in supercooled liquids is spatially heterogeneous on time scales shorter than $3\tau_\alpha$, which leads to the breakdown of the Stokes-Einstein relation.[6] The heterogeneity detected is essentially the same as that of the bond breakage in our former works [4,5].

In the present study, we examined the microscopic dynamics of a two-dimensional supercooled liquid under shear. The numerical analysis illustrated several interesting features such as (i) drastic reduction of relaxation times and the viscosity (ii) almost isotropic relaxation irrespective of the direction of the flow. The fact that the dynamics are almost isotropic supports the simplified view of sheared supercooled liquids proposed so far. In this

view, the effect of shear is transformed into scalar parameters, such the effective temperature, and the anisotropic nature of the nonequilibrium states is not explicitly considered[15,25].

Acknowledgments

The author would like to thank Prof. A. Onuki, Prof. D.R. Reichman, and Dr. K. Miyazaki for their collaborations and helpful discussions. Numerical calculations have been carried out at the Human Genome Center, Institute of Medical Science, University of Tokyo.

References

1. T. Muranaka, Y. Hiwatari: Phys. Rev. E **51**, R2735 (1995); Prog. Theor. Phys. Suppl. **126**, 403 (1997)
2. M.M. Hurley, P. Harrowell: Phys. Rev. E **52**, 1694 (1995)
3. D.N. Perera, P. Harrowell: Phys. Rev. E **54**, 1652 (1996)
4. R. Yamamoto, A. Onuki: J. Phys. Soc. Jpn. **66**, 2545 (1997)
5. R. Yamamoto, A. Onuki: Phys. Rev. E **58**, 3515 (1998)
6. R. Yamamoto, A. Onuki: Phys. Rev. Lett. **81**, 4915 (1997)
7. W. Kob, C. Donati, S.J. Plimton, P.H. Poole, S.C. Glotzer: Phys. Rev. Lett. **79**, 2827 (1997)
8. C. Donati, J.F. Douglas, W. Kob, S.J. Plimton, P.H. Poole, S.C. Glotzer: Phys. Rev. Lett. **80**, 2338 (1998)
9. P. Ray, K. Binder: Europhys. Lett. **27** 53 (1994)
10. C. Dasgupta, A.V. Indrani, S. Ramaswamy, M.K. Phani: Europhys. Lett. **15**, 307 (1991)
11. J. H. Simmons, R. K. Mohr, C. J. Montrose: J. Appl. Phys. **53**, 4075 (1982); J. H. Simmons, R. Ochoa, K. D. Simmons: J. Non-Cryst. Solids **105**, 313 (1988). Y. Yue R. Brückner: J. Non-Cryst. Solids **180**, 66 (1994)
12. R. Yamamoto, A. Onuki: Europhys. Lett. **40**, 61 (1997)
13. R. Yamamoto, A. Onuki: J. Chem. Phys. **117**, 2359 (2002)
14. A. J. Liu, S. R. Nagel: Nature **396**, 21 (1998)
15. J.-L. Barrat, L. Berthier: Phys. Rev. E **63**, 012503 (2001); L. Berthier, J.-L. Barrat: Phys. Rev. Lett. **89**, 095702 (2002); L. Berthier, J.-L. Barrat: J. Chem. Phys. **116**, 6228 (2002)
16. I.K. Ono, C.S. O'Hern, D.J. Durian, S.A. Langer, A.J. Liu, S.R. Nagel: Phys. Rev. Lett. **89**, 095703 (2002)
17. A. Onuki, K. Kawasaki: Ann. Phys. (N.Y.) **121**, 456 (1979); A. Onuki, J. Phys.: Condens. Matter **9**, 6119 (1997)
18. A. Onuki: *Phase Transition Dynamics* (Cambridge University Press, Cambridge 2002)
19. K. Miyazaki, D. R. Reichman: Phys. Rev. E **66** 050501 (2002)
20. K. Miyazaki, D. R. Reichman, R. Yamamoto: cond-mat/0401528, Phys. Rev. E (submitted)
21. D. J. Evans, G. P. Morriss: *Statistical Mechanics of Nonequilibrium Liquids* (Academic, New York 1990)

22. A similar but slightly different definition for $Fs(\mathbf{k}, t)$ was given in [5]. We however confirmed that the both definitions give almost identical results for the present case.
23. D. Ronis: Phys. Rev. A **29**, 1453 (1984)
24. G. Szamel: J. Chem. Phys. **114**, 8708 (2001)
25. M. Fuchs, M. E. Cates: Phys. Rev. Lett. **89**, 248304 (2002); F. Matthias, M. E. Cates: J. Phys.: Condens. Matter **15**, S401 (2003); F. Matthias, M. E. Cates: Faraday Discuss. **123**, 267 (2003)